RSC Advances

ROYAL SOCIETY OF CHEMISTRY

www.rsc.org/advances

Journal Name

RSCPublishing

COMMUNICATION

SnO_2 decorated graphene nanocomposite anode materials prepared via an up-scalable wet-mechanochemical process for sodium ion battery

Cite this: DOI: 10.1039/x0xx00000x

Received 00th January 2012,
Accepted 00th January 2012

DOI: 10.1039/x0xx00000x

www.rsc.org/

Sheng Li[a], Yazhou Wang[a], Jingxia Qiu[a], Min Ling[a], Haihui Wang[b], Wayde Martens[c], Shanqing Zhang[a]*

A facile and up-scalable wet-mechanochemical process is designed for fabricating ultra-fine SnO_2 nanoparticles anchored on graphene networks for use as anode materials for sodium ion batteries. A hierarchical structure of the SnO_2@graphene composite is obtained from the process. The resultant rechargeable SIBs achieved high rate capability and good cycling stability.

Introduction

Rechargeable batteries are not only important to satisfy our energy requirements in daily life, but also vital to address the emerging environmental issues and the world energy crisis. In the last decade, lithium ion batteries (LIBs) have achieved remarkable progress in electronic appliance applications and electrical vehicles[1-5]. However, large-scale applications of LIBs have been heavily restricted by their high cost and limited supply of lithium on the earth. In this regard, sodium ion batteries (SIBs) are considered as one of the most promising alternatives to LIBs, due to their significantly lower cost and the abundance of sodium. This is especially true in the smart grid applications where large scale, long term stability and low cost are the dominant factors[6-8]. Though LIBs and SIBs share similar chemistry in the charge/discharge processes, the essential components of LIBs cannot be simply adopted for SIBs owing to Na ion is substantially larger (55 % in radius) compared to the Li ion. For instance, graphite, the most commonly used LIBs anode material, is not suitable for SIBs due to its poor Na ion insertion property[9-11]. The electrode materials for SIBs should contain large and abundant transport channels for Na ions transportation.

Nevertheless, several anode materials such as carbon, alloys, metal sulfates and metal oxides have been investigated for SIBs[7, 12-21]. Among them, SnO_2 is one of the most promising candidates due to its high theoretical specific capacity of 667 mAh/g[18, 22]. In order to achieve the full capacity, the inherent deficiencies of SnO_2, such as poor electronic conductivity, and severe volume change during the charge/discharge processes which causes pulverization of the electrode and needs to be addressed[8, 23]. Mounting small SnO_2 particles on a resilient conductive substrate could be an effective strategy to tackle the above limitations. In this regard, graphene could benefit the entire battery process as it possesses superior conductivity, good mechanical strength, large surface area and unique sheet structure[21, 24].

In this work, a wet-mechanochemical method is designed for fabricating uniform SnO_2@graphene nanocomposites from $SnCl_2$ and graphene oxide (GO) which are ball-milled in aqueous media. Compared with other multi-step sophisticated methods[8, 22, 25, 26], this strategy is simple, rapid, facile, economical and most importantly up-scalable. The precursors ($SnCl_2$ and GO) are firstly dispersed homogeneously in water, before the constant and powerful mechanical striking of the milling media constrains Sn^{2+} at the surface of GO sheets where redox reactions are initiated by the high impact energy. As a result, GO is reduced to graphene while Sn^{2+} is oxidized to SnO_2, as shown in Eqn (1):

$$SnCl_2 + GO + H_2O \xrightarrow{\textbf{wet ball-milling}} SnO_2@graphene + HCl \quad (1)$$

Due to the necessity of both an oxidant and a reductant, only the impacts at the surface of the GO will result in successful reactions which producing in SnO_2 particles strongly bonded to the surface of the graphene. The random and high frequency nature of the impacts on the surface of GO ensure a relatively even SnO_2 coating. It is expected that a hierarchical SnO_2@graphene structure would form in this process which is beneficial to electrochemical performances of SIBs. Moreover, with the uniform coating, graphene sheets could be avoided from stacking together, enabling the efficient transportation in the electrode of Na ions.

Experimental

$SnCl_2 \cdot 2H_2O$ (0.45 g, Merck Pty. Ltd.) and graphene oxide (GO, 0.1 g, Tianjin Plannano Technology Co. Ltd.) are firstly dispersed in 10 mL deionized water. The resultant mixture is added to a planetary zirconia ball miller at room temperature at a speed of 500 rpm for 3 h. Then the as-prepared product SnO_2@graphene is washed in water and ethanol in sequence, and subsequently dried in a vacuum oven at

60 °C. Commercial tin oxide nanopowder (SnO_2, Nanostructured & Amorphous Materials Inc.) was used as a control sample.

The morphology was examined by a scanning electron microscope (SEM, JSM-7001F) and transmission electron microscopy (TEM, FEI Model Tecnai G20). X-ray diffraction (XRD) was also tested using CuKα radiation over the 2θ range of 10-80° (Model LabX-6000, Shimadzu, Japan). The multipoint Brunauer–Emmett–Teller (BET) surface area was estimated using adsorption data obtained from a surface area analyser (Micromeritics Tristar 3020). For X-ray photoelectron spectroscopy (XPS, Kratos Axis ULTRA incorporating a 165 mm hemispherical electron energy analyzer) test, all binding energies were referenced to the C1s peak (284.8 eV). Raman spectra were examined at room temperature by a Renishaw 100 system (Raman spectrometer using 514 nm Argon green laser as light source).

As active materials, the samples are mixed with 10 wt % carbon black and 10 wt% polyvinylidene difluoride (PVDF, Aldrich) in N-methyl-2-pyrrolidone (NMP, Aldrich) solvent to form homogeneous slurries. The resultant slurries are uniformly coated onto Cu foils with an area of 1 cm^2. The loading of the electrode material is c.a. 1~2 mg. The pasted Cu foils are dried in a vacuum oven at 60 °C and then pressed by a double-roll compressor. CR2032 coin-type cells are assembled in an argon-filled M-Braun glove box. A glass fiber (GA-55) membrane is used as the separator, a sodium metal sheet as the counter electrode, and 1 M $NaClO_4$ in a 1:1 (v/v) mixture of ethylene carbonate (EC) and propylene carbonate (PC) as the electrolyte. To measure the electrochemical capacity and cycle life of the working electrodes, the cells are charged and discharged using LANDCT 2001A battery tester (Wuhan, PRC) in a voltage range from 0.01 to 2.5 V vs Na/Na^+. Cyclic voltammetry (CVs) were performed using a CHI 660D electrochemical workstation (CH Instrument, Shanghai, PRC). CVs were recorded between 2.5 V and 0.01 V at a scan rate of 0.1 mV s^{-1}, using the composite as the working electrode and a sodium sheet as both counter electrode and reference electrode. Electrochemical impedance spectroscopy (EIS) was also carried out in this two-electrode system with amplitude of 5 mV over the frequency range from 100 kHz to 0.01 Hz.

Results and discussion

The SEM images in Fig. 1a and 1b display the morphologies of the GO and SnO_2@graphene samples, respectively. After wet ball-milling, the sheet-like shape of the graphene in SnO_2@graphene samples is maintained, but are now less-transparent, suggesting that the sheet thickness has been significantly increased, seemingly due to the SnO_2 nanoparticles anchored onto the graphene sheets. The anchored SnO_2 nano particles prevents the graphene sheets from stacking together, and the interlaced sheets would create some voids/channels in the electrode which are tolerant for the dramatic volume change during the charge/discharge process. The corresponding selected-area electron diffraction (SAED) pattern in Fig. 1c (inset) shows that the rings from inside to outside are well-indexed to the (100), (101), and (211) planes of SnO_2, respectively, confirming the formation of SnO_2. It can be observed that the SnO_2 particles are fine and uniform, densely attached on graphene sheets. The HRTEM images in Fig. 1d and S1 clearly show that the regular inter-plenary spacing of 0.34 nm can be ascribed to the (110) planes of SnO_2 and the average SnO_2 particle size is only *c.a.* 3 nm.

The XRD pattern in Fig. 2a confirms the formation of SnO_2 (PDF 41-1445). According to the Scherrer equation, the crystal diameter can be approximated as *c.a.* 3 nm, agreeing well with the results of HRTEM. Achieving such a small particle size can be considered as a unique advantage of the proposed wet mechanochemical method as the dry mechanochemical method can commonly achieve as small as several micrometres[27]. This ultra-fine size would be beneficial to Na ions mass transport as it shortens the diffusion path length of the Na ions. The adsorption–desorption isotherms belong to type IV based on the hysteresis loop (Fig. 2b), which indicates the existence of 3-D channels and the network structure. The SnO_2@graphene composites exhibit a high surface area of 273 m^2/g according to the BET measurement. This also implies successful inhibition to the aggregation of nanoparticles and restacking of graphene sheets, which may enable the insertion/extraction of Na ions for the graphene sheets. The weight percentage of SnO_2 of the composites is characterizes by TGA test as c.a. 70%.

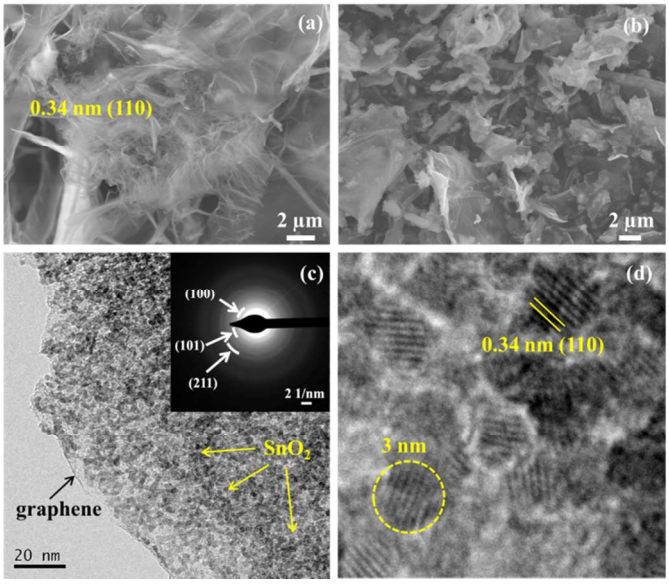

Fig. 1 (a) SEM image of the GO; (b) SEM image of SnO_2@graphene; (c) TEM image with the SAED pattern (inset) of SnO_2@graphene and (d) HR-TEM image of SnO_2@graphene sample.

The reduction degree of GO by reaction (1) was investigated by XPS measurements. Fig. 2c displays the data of C *1s* for GO and SnO_2@graphene samples. The oxygen functional groups could be clearly observed from GO profile, which are corresponding to C*-CO, C-O, C=O and COOH, respectively[24]. In comparison, for SnO_2@graphene, after the wet ball-milling process, the oxygen functional groups on the surface of graphene decreased dramatically, indicating the successful reduction from GO to graphene. The color of the samples also changes from brown to black as shown in Fig. 2e, suggesting the successful reduction of GO. D band and G band peaks could be observed in Raman spectra (Fig. 2d) for both the SnO_2@graphene composite and GO. It is established that the ratio of the D band and G band intensities (I_D/I_G) reflects the extent for the disruption of the symmetrical hexagonal graphitic lattice[28-30]. In this case, the I_D/I_G for SnO_2@graphene is higher than that of GO due to the interaction of the between SnO_2 and graphene leads to the disruption. This implies that the SnO_2 nano particles are successfully anchored on graphene sheets.

Electrochemical characteristics of the commercial SnO_2 and SnO_2@graphene samples were investigated systematically as anodes of SIBs. Fig. 3a and 3b present the CV curves of the commercial

SnO_2 and SnO_2@graphene samples with a scan rate of 0.1 mV/s. At the first cycle of SnO_2 electrode, three obvious irreversible cathodic peaks could be observed at 0.75 V, 0.4 V and 0.01V, which are attributed to the formation of $NaSn_5$, NaSn and Na_xSn_4 ($x \geq 9$), respectively, according to the density functional theory (DFT) calculation results for the Sn sodiation voltages of SIBs[31].

$$SnO_2 \rightarrow Sn \rightarrow NaSn_5 \rightarrow NaSn \rightarrow Na_9Sn_4 \rightarrow Na_{15}Sn_4. \quad (2)$$

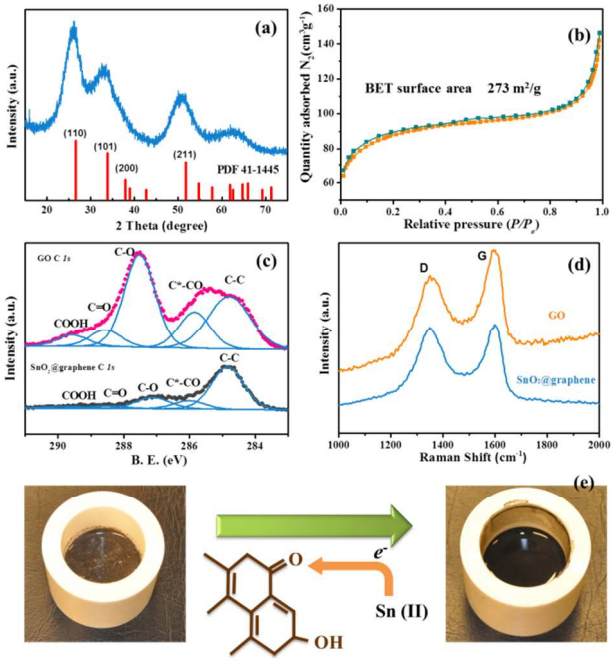

Fig. 2 (a) XRD image and (b) BET adsorption measurement of the SnO_2@graphene; (c) XPS of C 1s for GO and SnO_2@graphene samples; (d) Raman spectra of SnO_2@graphene sample and GO. (e) The reaction mechanism and the colours of reactants and products

In contrast, the CV curve of the first cycle for SnO_2@graphene (Fig. 3b) shows only a cathodic broad peak at 0.01~0.4 V which is contributed by the reduction for SnO_2 nanoparticles to $Na_{15}Sn_4$, the formation of solid electrolyte interface (SEI) and the insertion of Na ions into graphene 3-D network. The shapes of the CV curves in the following two cycles are similar as the first one. It can be concluded as the capacity of SnO_2@graphene for SIBs is a combination of two parts: the insertion/extraction of Na ion in graphene 3-D framework and the alloying/dealloying between Sn and $Na_{15}Sn_4$. It can be described as equations (3), (4) and (5)[8, 22]:

$$SnO_2 + 4Na^+ + 4e^- \rightarrow Sn + 2Na_2O \quad (3)$$

$$4Sn + 15Na^+ + 15e^- \leftrightarrow 4Na_{15}Sn_4 \quad (4)$$

$$C + xNa^+ + xe^- \leftrightarrow Na_xC \quad (5)$$

The shapes of CV profile for SnO_2@graphene sample is quite similar as the shapes of carbon material[32], but the capacity is much higher than that of graphene sample (about 176 mAh/g at 0.1 A/g[33]).

The charge/discharge voltage profiles of the commercial SnO_2 and SnO_2@graphene samples are evaluated at 0.1 A/g in the range of 0.1~2.5 V as shown in Fig. 3c. A characteristic irreversible discharge plateau from 0.8 V vs. Na^+/Na is observed and the resultant electrode delivers a high specific capacity at 750 mAh/g at the 1st cycle while it maintains only 407 mAh/g at the 2nd cycle due to the irreversible reactions at the first cycle, agreeing well with the CV result. From the 2nd cycle, this plateau disappears, and the charge/discharge curves almost overlap, indicating that the electrochemical reduction process is completed since the reduction reaction of SnO_2 is an irreversible reaction[18] and the SEI is stabilized.

In comparison with the control sample, the SnO_2@graphene shows a lot better cycling stability as shown in Fig. 3d. After 50 cycles, the capacity of the SnO_2@graphene is 286 mAh/g and maintains at 270 mAh/g after 100 cycles (86% retention for the 5th cycle). Interestingly, the extraordinary coulombic efficiencies (>100%) are observed in first 3 cycles mainly due to due to there is an irreversible discharge process, (Reaction (3)) in addition to the reversible discharge process (Reaction (4)). After 3 cycles, the charge/discharge capacities stabilize and the coulombic efficiency continuously maintain at ca. 100%, showing a good reversibility. The commercial SnO_2 only delivers a low initial irreversible discharge capacity (315 mAh/g) and then drops rapidly to zero.

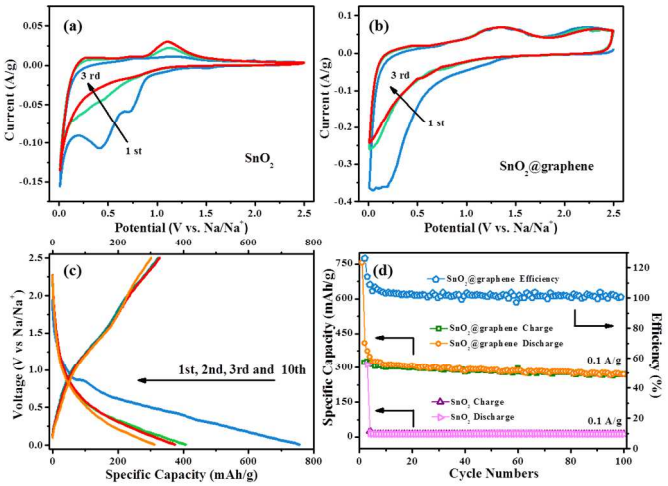

Fig. 3 (a) CV profiles for the first 3 cycles of commercial SnO_2 sample and (b) SnO_2@graohene sample as the electrodes materials for SIBs. (c) The charge/discharge profiles for the SnO_2@graphene SIB; and (d) the charge/discharge capacities and the coulombic efficiency of the SnO_2@graphene and the capacities of the commercial SnO_2 at a current density of 0.1 A/g

The rate capacities of the SnO_2@graphene samples are further investigated in Fig. 4a. The SnO_2@graphene delivers a discharge capacity of 320 mAh/g at a current density of 0.05 A/g. When the rate rises to 0.1, 0.2, 0.4 and even 0.8 A/g, the specific capacities are retained and are quantified as 290, 274, 246 and 207 mAh/g, respectively. An excellent rate capability and stability was observed in that only 28.6% capacity loss when the rates increase from 0.1 to 0.8 A/g. The high rate capacity (0.8 A/g) for the SnO_2@graphene composites is among the best of current literatures[8, 18, 25], which is due to the small particle size of SnO_2 and the special networks structure with a large specific area. After the varied rate cycles, the capacity of the electrode could nearly recover to the initial capacity of over 285 mAh/g at 0.1 A/g. Fig. 4b presents the charge and discharge profiles of SnO_2@graphene for SIB at different current densities. It could be observed that with the increase of the current

density, the curves shape does not change, suggesting the SnO_2@graphene electrode can enable a fast transportation of Na ions for SIBs. The structure and the chemistry during the charge and discharge process are all stabilized, which is benefited from the framework structure of the electrode.

EIS measurements are conducted for the SnO_2@graphene and SnO_2 control samples after 3 cycles charge/discharge. Both of the Nyquist plots shown in Fig. 4c display depressed semicircles in high-middle frequency region, which are ascribed to the charge transfer resistance (R_{ct}, directly proportional to the radius of the semicircles); and a 45° inclined line in the low frequency region, which can be considered to be Warburg impedance. A much smaller R_{ct} (~ 20 Ω for SnO_2@graphene; ~ 338 for commercial SnO_2) could be observed for the SnO_2@graphene, which can be attributed to robust and strong links between the SnO_2 and graphene sheets as well as the highly conductive nature of the graphene.

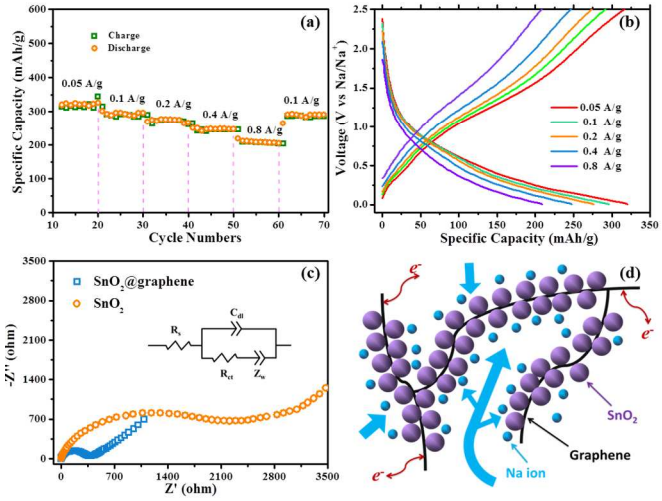

Fig. 4 (a) the rate charge/discharge capability for SnO_2@graphene and (b) their charge and discharge curves from 0.05 A/g to 0.8 A/g (from the 15th, 25th, 35th, 55th cycles, respectively), (c) Nyquist plots of the SnO_2@graphene and commercial SnO_2. (d) Schematic representation of the hierarchical structure of the SnO_2@graphene nanocomposite for SIBs.

The mechanism responsible for the exceptional electrochemical performance and resilient stability of the resultant SIBs can be concluded in Fig. 4d. Firstly, the achievement of ultra-small size of the SnO_2 particles (*c.a.* 3 nm), the successful prevention of the graphene stacking and the strong links between the SnO_2 and graphene sheets facilitate thorough electrochemical reduction of SnO_2 for Sn production. Secondly, the superior electronic conductivity of graphene, produced by the thorough reduction reaction of GO in the wet-mechanochemical process, which guarantees high electron collection percentage within the 3-D network. Last but not least, such robust 3-D conductive networks and the hierarchical structure of the nanocomposites would accommodate the dramatic volume change of SnO_2 and Sn during charge/discharge progress. Large surface areas and channels in the electrode not only enhance rapid mass transport of the Na ions within the resultant 3-D networks and the alloying/dealloying process, but also enables the insertion and extraction of Na ions in graphene sheets.

Conclusions

SnO_2@graphene nanocomposites are successfully synthesized via a facile wet-mechanochemical route. The SnO_2 nanoparticles are uniformly anchored onto graphene sheets, forming a hierarchical 3-D network on the electrode. This process prohibits the aggregation of SnO_2, eliminates the restacking of graphene sheets and therefore enhances the mass transport of Na ions within the 3-D conductive graphene network. Consequently, the SnO_2@graphene composite could overcome the problems of pulverization and high resistance of SnO_2, delivering outstanding energy capacity and cycling stabilities in SIBs. This process is a promising way for mass production of low cost and high quality anode materials for SIBs.

Acknowledgements

The authors acknowledge the financial supports from Australia Research Council and Griffith University, Australia, and the facilities and the scientific and technical assistance of the Australian Microscopy & Microanalysis Research Facility at the Center for Microscopy and Microanalysis (CMM) at the University of Queensland, Australia.

Notes and references

[a] Centre for Clean Environmental and Energy, Environmental Futures Research Institute, and Griffith School of Environment, Griffith University, Gold Coast, QLD 4222, Australia
[b] College of Chemistry and Chemical Engineering, South China University of Technology, Guangzhou 510640, China
[c] Discipline of Nanotechnology and Molecular Science, Queensland University of Technology, GPO Box 2434, Brisbane, Queensland 4001, Australia
E-mail: s.zhang@griffith.edu.au;
Tel: +61-7-5552-8155
Electronic Supplementary Information (ESI) available: further characterizations of TEM and Raman tests. See DOI: 10.1039/b000000x/

1. J. Qiu, S. Li, E. Gray, H. Liu, Q.-F. Gu, C. Sun, C. Lai, H. Zhao and S. Zhang, *J. Phys. Chem. C*, 2014, **118**, 8824.
2. J. B. Goodenough and K. S. Park, *J. Am. Chem. Soc.*, 2013, **135**, 1167.
3. B. Guo, Y. Li, Y. Yao, Z. Lin, L. Ji, G. Xu, Y. Liang, Q. Shi and X. Zhang, *Solid State Ionics*, 2011, **204–205**, 61.
4. M. Ling, J. Qiu, S. Li, G. Liu and S. Zhang, *J. Mater. Chem. A*, 2013, **1**, 11543.
5. J. Qiu, C. Lai, S. Li and S. Zhang, *RSC Adv.*, 2014, **4**, 18899.
6. T. Chen, Y. Liu, L. Pan, T. Lu, Y. Yao, Z. Sun, D. H. C. Chua and Q. Chen, *J. Mater. Chem. A*, 2014, **2**, 4117.
7. J. Qian, X. Wu, Y. Cao, X. Ai and H. Yang, *Angew. Chem., Int. Ed.*, 2013, **52**, 4633.
8. D. Su, H. J. Ahn and G. Wang, *Chem. Commun.*, 2013, **49**, 3131.
9. M. D. Slater, D. Kim, E. Lee and C. S. Johnson, *Adv. Funct. Mater.*, 2013, **23**, 947.
10. S.-W. Kim, D.-H. Seo, X. Ma, G. Ceder and K. Kang, *Adv. Energy Mater.*, 2012, **2**, 710.
11. V. Palomares, P. Serras, I. Villaluenga, K. B. Hueso, J. Carretero-González and T. Rojo, *Energy Environ. Sci.*, 2012, **5**, 5884.
12. X. Zhou and Y.-G. Guo, *ChemElectroChem*, 2014, **1**, 83.

13. Y. Shao, J. Xiao, W. Wang, M. Engelhard, X. Chen, Z. Nie, M. Gu, L. V. Saraf, G. Exarhos, J. G. Zhang and J. Liu, *Nano Lett.*, 2013, **13**, 3909.
14. C. W. Mason, I. Gocheva, H. E. Hoster and D. Y. Yu, *Chem. Commun.*, 2014, **50**, 2249.
15. H. Xiong, M. D. Slater, M. Balasubramanian, C. S. Johnson and T. Rajh, *J. Phys. Chem. Lett.*, 2011, **2**, 2560.
16. S. Yuan, X. L. Huang, D. L. Ma, H. G. Wang, F. Z. Meng and X. B. Zhang, *Adv. Mater.*, 2014, **26**, 2273.
17. C. Deng, S. Zhang, Z. Dong and Y. Shang, *Nano Energy*, 2014, **4**, 49.
18. Y.-X. Wang, Y.-G. Lim, M.-S. Park, S.-L. Chou, J. H. Kim, H.-K. Liu, S.-X. Dou and Y.-J. Kim, *J. Mater. Chem. A*, 2014, **2**, 529.
19. L. Xiao, Y. Cao, J. Xiao, W. Wang, L. Kovarik, Z. Nie and J. Liu, *Chem. Commun.*, 2012, **48**, 3321.
20. P. Senguttuvan, G. Rousse, V. Seznec, J.-M. Tarascon and M. R. Palacín, *Chem. Mater.*, 2011, **23**, 4109.
21. Z. Jian, B. Zhao, P. Liu, F. Li, M. Zheng, M. Chen, Y. Shi and H. Zhou, *Chem. Commun.*, 2014, **50**, 1215.
22. Y. Wang, D. Su, C. Wang and G. Wang, *Electrochem. Commun.*, 2013, **29**, 8.
23. H. Zhu, Z. Jia, Y. Chen, N. Weadock, J. Wan, O. Vaaland, X. Han, T. Li and L. Hu, *Nano Lett.*, 2013, 3093.
24. S. Li, Y. Wang, C. Lai, J. Qiu, M. Ling, W. N. Martens, H. Zhao and S. Zhang, *J. Mater. Chem. A*, 2014, **2**, 10211.
25. Y. Xu, Y. Zhu, Y. Liu and C. Wang, *Adv. Energy Mater.*, 2013, **3**, 128.
26. C. Gu, H. Zhang, X. Wang and J. Tu, *Mater. Res. Bull.*, 2013, **48**, 4112.
27. C. Lai, Z. Wu, Y. Zhu, Q. Wu, L. Li and C. Wang, *J. Power Sources*, 2013, **226**, 71.
28. C. Zhong, J. Wang, Z. Chen and H. Liu, *J. Phys. Chem. C*, 2011, **115**, 25115.
29. Y.-H. Hwang, E. G. Bae, K.-S. Sohn, S. Shim, X. Song, M. S. Lah and M. Pyo, *J. Power Sources*, 2013, **240**, 683.
30. J. Liang, W. Wei, D. Zhong, Q. Yang, L. Li and L. Guo, *ACS Appl. Mater. Interfaces*, 2012, **4**, 454.
31. V. L. Chevrier and G. Ceder, *J. Electrochem. Soc.*, 2011, **158**, A1011.
32. T. Chen, L. Pan, T. Lu, C. Fu, D. H. C. Chua and Z. Sun, *J. Mater. Chem. A*, 2014, **2**, 1263.
33. Y.-X. Wang, S.-L. Chou, H.-K. Liu and S.-X. Dou, *Carbon*, 2013, **57**, 202.

Graphical Abstract

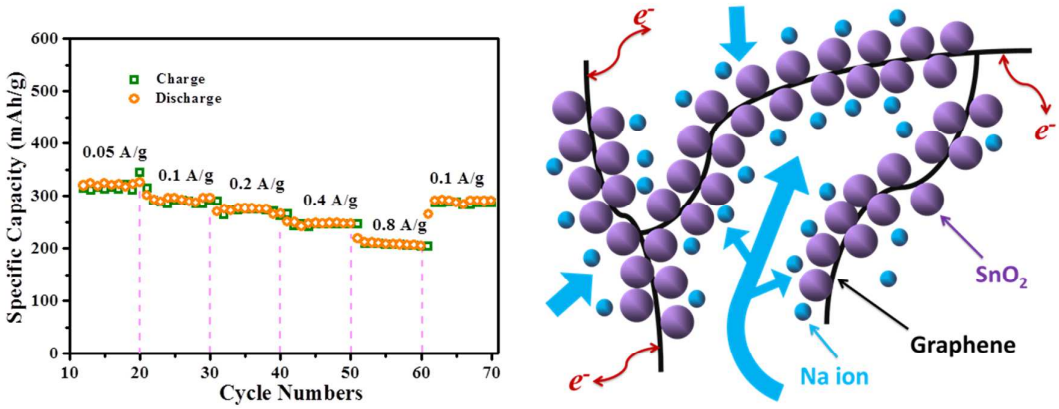

A hierarchical structured SnO_2@graphene nanocomposite has been obtained with superior high-rate and cycle performance for sodium ion battery.